

See discussions, stats, and author profiles for this publication at: <https://www.researchgate.net/publication/228674318>

# Controlling the Morphology of BaCO<sub>3</sub> Aggregates by Carboxymethyl Cellulose through Polymer Induced Needle-Stacking Self-Assembly

ARTICLE in CRYSTAL GROWTH & DESIGN · JUNE 2010

Impact Factor: 4.89 · DOI: 10.1021/cg100159k

---

CITATIONS

18

---

READS

17

## 4 AUTHORS, INCLUDING:



Shengtong Sun

Universität Konstanz

27 PUBLICATIONS 650 CITATIONS

[SEE PROFILE](#)



Peiyi Wu

Fudan University

218 PUBLICATIONS 3,630 CITATIONS

[SEE PROFILE](#)

# Controlling the Morphology of BaCO<sub>3</sub> Aggregates by Carboxymethyl Cellulose through Polymer Induced Needle-Stacking Self-Assembly

Wei Li, Shengtong Sun, Qisi Yu, and Peiyi Wu\*

*Key Laboratory of Molecular Engineering of Polymers (Ministry of Education), Laboratory of Advanced Materials, Department of Macromolecular Science, Fudan University, Shanghai 200433, People's Republic of China*

Received February 2, 2010; Revised Manuscript Received April 5, 2010

**ABSTRACT:** Inspired by mineralization in biological organisms, fabrication of higher ordered inorganic crystals induced by polymer chains has received much attention. In our present work, we made use of a widely used industrial material, carboxymethyl cellulose (CMC), to mediate the nucleation and growth of barium carbonate (BaCO<sub>3</sub>). We calculated the interactions between CMC chains and crystalline needle-like units of BaCO<sub>3</sub> by molecular dynamic simulation, concluding that the (111) face of crystalline units is the most favorable face for CMC chains to attach onto. Based on the simulation results and the time-resolved experiments, we suggested the dumbbell-like BaCO<sub>3</sub> aggregates formed via polymer induced stacking of needle-like units. More importantly, we realized control over the morphology of aggregates from dumbbell-like to spherical particles by simply adjusting the polymer concentration. By clarifying the aggregation mechanism mediated by polymer chains, we demonstrate here not only a simple method to fabricate BaCO<sub>3</sub> particles with controllable morphologies but also a reference work which may serve the exploration of the mechanism in biomimetic mineralization.

## 1. Introduction

Fabrication of higher ordered inorganic crystals by a self-assembly process has received much attention not only for its importance on crystallization theories but also for the potential to design new materials used in many fields, such as catalysis, electronics, and ceramics.<sup>1–4</sup> As a common process throughout nature and technology, self-assembly involves components from molecular to planetary scale.<sup>4</sup> For example, biological systems take use of organic templates to regulate the synthesis of biominerals with hierarchical structures and profound functions including protection and structural support, such as bones and shells.<sup>5,6</sup> Nacreous layers constructed with brick-and-mortar structure endow the shell with excellent mechanical properties,<sup>7</sup> which inspired amounts of studies on biomimetic synthesis of organic/inorganic composites with such hierarchical structures.<sup>8,9</sup> Regulated by organic templates, such biominerals are definitely not formed by the classical ion-by-ion crystallization route.<sup>10</sup> Based on the mineralization process in organisms and *in vitro* biomimetic experiments, Colfen et al.<sup>11,12</sup> developed the nonclassical crystallization mechanism: all crystalline structures, even single crystals, can be formed by aggregation of subunits with a difference in the degree of orientation, followed by a fusing process of the building units, in which organic templates played important roles.

Carbonate minerals, including CaCO<sub>3</sub>, BaCO<sub>3</sub>, and SrCO<sub>3</sub>, were intensively studied as model compounds for biomimetic mineralization, among which CaCO<sub>3</sub> was most researched because of the important role it plays in various kinds of biominerals, such as shells and eggshells, as well as its wide usage in many industrial aspects, including paints, papermaking, and the rubber industry, etc.<sup>6,13</sup> It has been shown that the aggregation method and, thus, the structure and morphology of CaCO<sub>3</sub> can be effectively controlled by using

soluble additives such as synthetic polymers,<sup>13</sup> proteins,<sup>14,15</sup> and polysaccharides.<sup>16</sup> In comparison, research on BaCO<sub>3</sub> was relatively less probably due to its rare existence in biological systems. However, considering the important applications of BaCO<sub>3</sub> in the glass and ceramic industries as well as its use as a precursor for magnetic ferrites,<sup>2</sup> it is necessary to study the crystallization of BaCO<sub>3</sub> in detail. Moreover, studying the mechanism of BaCO<sub>3</sub> formation may help us understand the crystallization of minerals regulated by organic additives and further uncover the still unclear mechanism of biomimetic mineralization due to the close structural similarity between witherite and aragonite, which is the principle inorganic component in the pearl layer. Xu and Colfen<sup>1</sup> have utilized a double hydrophilic block copolymer to control the crystallization of barium carbonate and formed self-organized dynamic structure patterns. Yu et al.<sup>2,17–20</sup> have carried out a series of studies on BaCO<sub>3</sub> and obtained products with various morphologies, among which helical BaCO<sub>3</sub> fibers are the most interesting<sup>17,20</sup> because the helical alignment of nanofibers can be induced by racemic polymers through selective adsorption on specific crystal faces. In their works, they constructed needle-like BaCO<sub>3</sub> units by molecular dynamic simulation and predicted the favorable polymer adsorption sites during the aggregation. Actually, computational techniques at the organic–inorganic interface in biomimetic mineralization have been intensively developed recently.<sup>21</sup> Researchers have studied the nucleation and growth process of CaCO<sub>3</sub> mediated by additives with atomistic models including molecular dynamic simulation.<sup>22–24</sup> So herein, we start the investigation with the interactions between polymer chains and crystalline units by computational simulation and try to understand how the polymer additives affect the growth process, especially the aggregating process of crystalline units.

We utilized a water-soluble derivative of cellulose—carboxymethyl cellulose (hereafter CMC)—to conduct the nucleation and aggregation of BaCO<sub>3</sub>. CMC was frequently adopted as a

\*Corresponding author: E-mail: Peiyiwu@fudan.edu.cn.

kind of representative polyanion in polymeric and colloidal chemistry in the laboratory for its good biocompatibility.<sup>25–27</sup> More importantly, it was applied in many industrial branches, such as paper-coating, cosmetics, mineral processing, pharmaceuticals, and the adhesive industry.<sup>28</sup> Recently, we identified the hydrogen bond structures in CMC with spectroscopic and thermal analysis.<sup>29</sup> We further successfully utilized CMC to induce the crystallization of rosette-like calcite spherules and suggested that the crystals were formed via an unconventional rhombohedra-stacking route; that is, rhombohedral subunits aggregated in partial rather than complete superposition between each other due to the electrostatic repulsive interactions between the polyanion chains adsorbed on the blocks.<sup>30</sup> Compared with the traditional CO<sub>2</sub>-diffusion method, we developed the method via the carbonation route with compressed/supercritical CO<sub>2</sub>, in which the carbonation rate was much faster. Taking CMC chains as direct polymer skeletons, we obtained submicronic calcite particles with ellipsoidal morphology in size of hundreds of nanometers.<sup>31</sup> In our present work, we continue to take CMC chains as polymer additives to mediate the growth of BaCO<sub>3</sub>. First, the interactions between the organic and mineral phases were investigated by the method of molecular dynamic simulation. We determined the possible route by which polymer chains could affect the crystallization process and suggested the formation mechanism of BaCO<sub>3</sub> aggregates with dumbbell-like morphology, which may also serve the interpretation in other mineralization systems. Furthermore, we realized the control over the morphologies of the products by changing the aggregation manner of the needle-like units, which may have potential applications in the ceramic and glass industry.

## 2. Experimental Section

**Materials.** Barium chloride and ammonium carbonate were purchased from Sinopharm Chemical Reagent Co. Ltd. The sodium salt of carboxymethyl cellulose (NaCMC) was purchased from Acros with a molecular weight of 90,000 and degree of carboxyl substitution (DS) of 0.7. All of the above chemicals are of analytical grade and used without further purification. The water used in all experiments is deionized water (DIW).

**Crystallization of BaCO<sub>3</sub>.** All glassware (glass bottles and small pieces of glass substrates) was cleaned and sonicated in ethanol for 15 min, then rinsed with DIW, further soaked in a HNO<sub>3</sub>–H<sub>2</sub>O<sub>2</sub>–DIW (1:1:1) solution, then rinsed with DIW, and finally dried with acetone. The mineralization experiments were carried out with a CO<sub>2</sub>-diffusion method. Briefly, the mineralization experiment was performed in a vessel with a volume of 15 mL which was placed in a closed desiccator at room temperature (22 ± 2 °C). For a typical mineralization process, 10 mL of 0.5 g/L NaCMC solution with 0.01 M BaCl<sub>2</sub> was freshly prepared in a 15 mL vessel and covered with parafilm; the parafilm was then punctured with three needle holes, and the vessel was put in a closed desiccator with a bottle of crushed ammonium carbonate powder at the bottom. The reaction started as soon as the vessel was put into the desiccator. After different intervals, the vessel was taken out of the desiccator, the glass pieces were taken out, and the precipitate was rinsed with DIW and ethanol and dried under ambient conditions. The precipitate in the solution was separated by centrifuging and then rinsed with DIW three times and then dried under ambient conditions. Time-resolved experiments were performed by taking out the glass pieces at a set interval to stop the reaction.

**Characterization.** The transmission electron microscope (TEM) images were taken with a JEOL JEM 2011 at 200 kV equipped with electron diffraction. Scanning electron microscope (SEM) observations were performed on a TS5136MM microscope and the specimens were coated with gold, and field-emission SEM (FE-SEM) examinations were carried out on a Hitachi S-4800. X-ray powder diffraction data were recorded on an X'pert Pro with Cu Kα radiation.

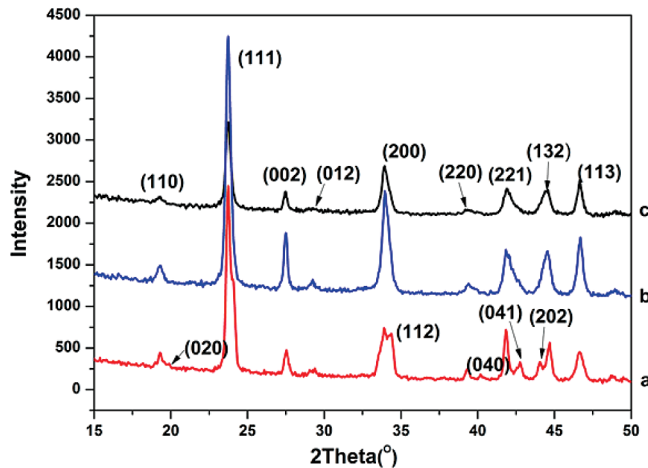


**Figure 1.** XRD patterns of BaCO<sub>3</sub> particles obtained in 0.01 g/L (a), 0.5 g/L (b), and 5 g/L (c) CMC solution, respectively. The XRD patterns depict the witherite phase of BaCO<sub>3</sub> (JCPDS 71-2394, orthorhombic, *Pmcn* space group).

**Molecular Dynamic Simulation.** Molecular structures of repeat units and chain segments of CMC in their amorphous state and the BaCO<sub>3</sub> cells and supercells were constructed with Materials Studio version 4.2 (Accelrys Inc., San Diego, CA, 2008). The energy optimization and molecular dynamics were accounted for by the COMPASS force field, which was implemented in the Forceit and Discover modules.

## 3. Results and Discussion

**3.1. Molecular Dynamic Simulation of Interaction between CMC Chains and BaCO<sub>3</sub> Supercells.** According to the repeat unit of CMC (the degree of carboxyl substitution of 0.7 was taken into consideration), the chain segment with 20 repeat units were constructed. The conformation of the segment is relatively rigid, which is consistent with the results calculated in the aqueous solution.<sup>32</sup> The final optimized conformation of the amorphous state was presented in Figure S1 of the Supporting Information.

We recorded the X-ray diffraction (XRD) patterns of BaCO<sub>3</sub> products obtained in CMC solutions with several different concentrations, as Figure 1 shows, which indicates that the obtained product is the witherite phase, subordinate to the orthorhombic phase and the *Pmcn* space group (JCPDS 71-2394). Based on the diffraction peaks and the simulation method Yu and Colfen adopted,<sup>20</sup> we built BaCO<sub>3</sub> nanocrystalline units (The lattice cell of BaCO<sub>3</sub> is shown in Figure S2 of the Supporting Information). To equal the volume size of the amorphous CMC cell and the witherite unit, we constructed the supercell (3\*3\*3) of witherite based on the primary lattice cell. Four main crystalline faces were cleaved along the planes (110), (111), (002), and (200) (see Figure S3 of the Supporting Information), and the interactions between amorphous CMC segments and these four faces were calculated, respectively. Taking the (111) plane as an example, we first put the polymer segment together with the supercell in the same space, and the initial state is that the CMC segment and supercell are apart from each other, as Figure 2a and b shows. With the simulation time extending, due to the interactions between the segment and the (111) plane (mainly electrostatic interaction), the CMC segment approached closer and closer to the crystal face, accompanied by the adjustment of its own chain conformations (Figure 2b–e). Finally, we observed that the segment attached

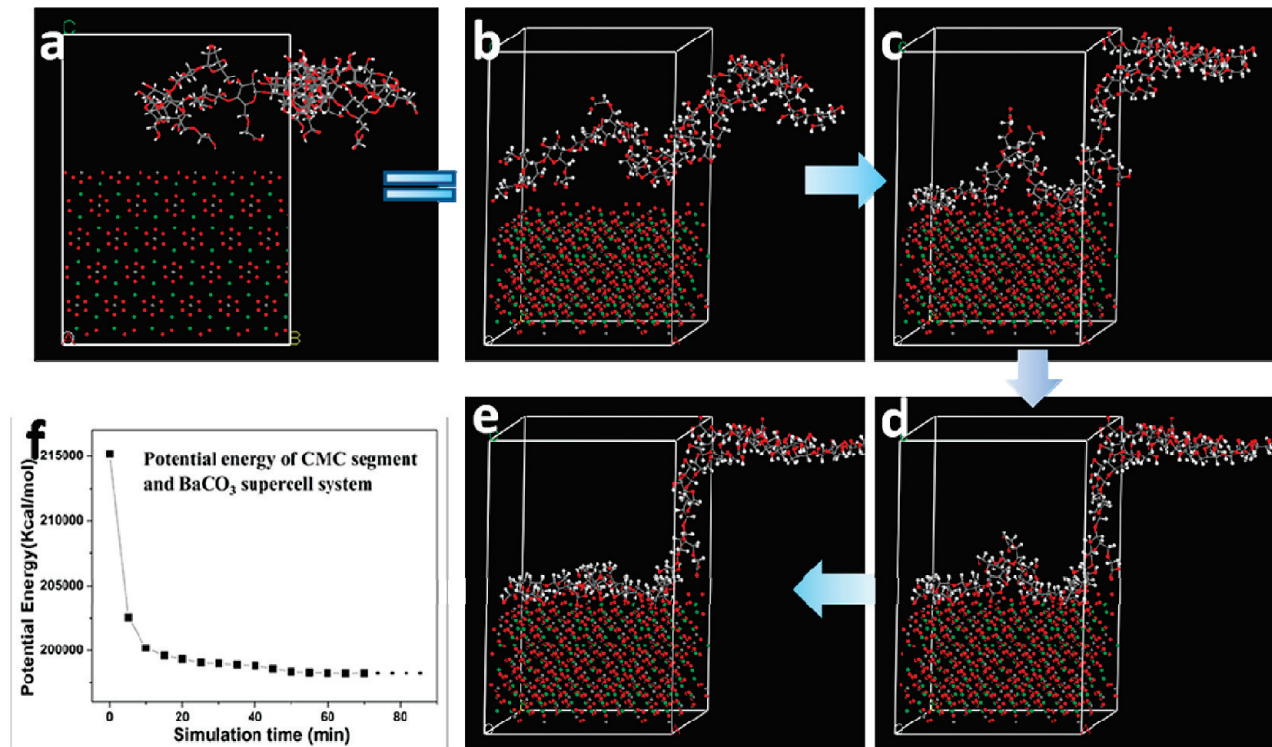


**Figure 2.** Initial state of the system of CMC segment and cleaved (111) plane (a and b). Process of the CMC segment approaching to the (111) face with the expanding simulation time (b–e). Plot of the system potential energy versus the simulation time (f).

**Table 1. Potential Energy When a CMC Segment Interacts with Four Different Crystal Planes**

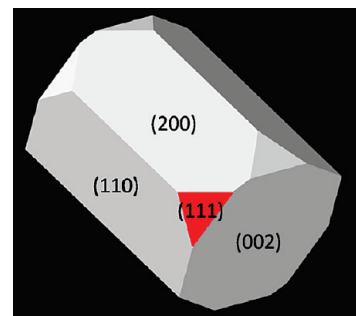
	potential energy for the following crystal planes (kcal/mol)			
	110	111	002	200
layers	26,154,168.6	3,034,934,647.1	24,819,107,719.8	316,290,935.5
supercell (witherite)	777,703.8	810,105.7	433,647.5	413,677.7
CMC interaction	25,376,464.8	3,034,124,776.8	24,818,674,009.1	315,877,298.1
	0	-235.4	63.2	-40.3

onto the face closely, and it could be found that the actual interacting layers were very thin. It should be noticed that the other half of the segment was similarly interacting with another (111) plane. During this process, the potential energy of the entire system decreased until it was close to a constant (Figure 2f), which indicated the equilibrium state of interaction between the organic and inorganic phases.

We calculated the potential energy when CMC segments interact with four different crystalline planes, including (110), (111), (002), and (200), respectively. The results are listed in Table 1. To identify the interaction between CMC segment and witherite supercell, we subtracted the sum of supercell and CMC energy from the layer's energy and obtained the interacting energies of four different faces, respectively. It was found that the relative sequential order among four faces was as follows: (111) < (200) < (110) < (002). That is to say, the (111) face of the witherite unit is the most favorable face for CMC segments to attach onto, while the (002) face is the most unfavorable one.

Based on the above simulation results, we presented the primary nanocrystalline witherite unit, as Scheme 1 shows. Among the interactions between crystalline units and polymers, the (111) face is the most accessible face to bind with polymers, which is marked as red in Scheme 1. In other words, despite the variation of the concentration of polymer, the most probable interaction site for CMC chains to bind

**Scheme 1. Primary Needle-like Nanocrystalline Units of Witherite<sup>a</sup>**



<sup>a</sup>The main crystal faces, including (110), (111), (002), and (200), were presented, and the (111) face was marked in red.

with the units is not the middle but the end of needle-like units, which set a foundation for our subsequent mechanistic interpretation of the morphological evolution of BaCO<sub>3</sub> aggregates.

**3.2. Growth Route of BaCO<sub>3</sub> Aggregates Induced by CMC Chains. 3.2.1. Aggregating Process in 0.1 g/L CMC Solution.** We first investigated the growth of BaCO<sub>3</sub> in CMC aqueous solution with a 0.1 g/L concentration. Quasi-time-resolved experiments were performed to trace the morphological evolution of the products, and typical electron micrographs

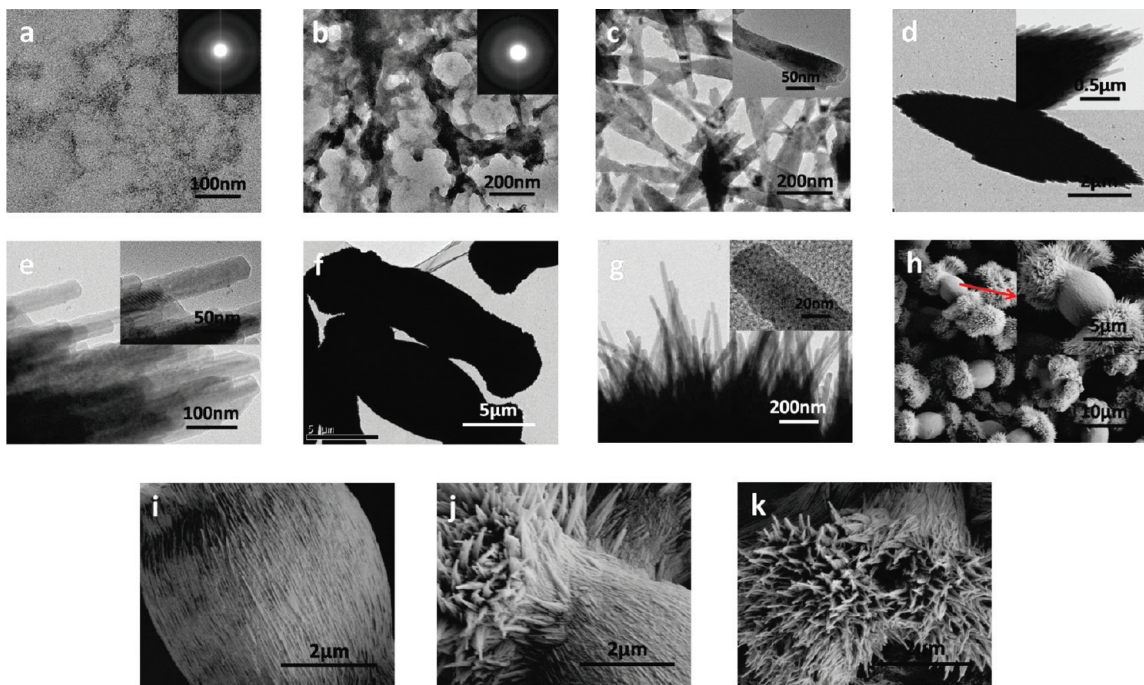


**Figure 3.** TEM images of  $\text{BaCO}_3$  products grown in 0.1 g/L CMC solutions after a reaction time of 15 min (a), 30 min (b), 1 h (c), 2 h (d, e), and 4 h (f, g), respectively. The insets of parts a and b are the ED patterns performed at the corresponding area, and the insets of parts c, d, e, and g are the enlarged images. FESEM images of  $\text{BaCO}_3$  products grown in 0.1 g/L CMC solutions after reaction times of 12 h (h), (i), (j), and (k), and the inset of part h is the enlarged image of an individual particle.

were presented in Figure 3. At the very early stage of reaction (15 min), as in many mineralization systems of  $\text{CaCO}_3$ ,<sup>33,34</sup> amorphous  $\text{BaCO}_3$  products were generated, which was confirmed by energy dispersive X-ray (EDX) spectra (Figure S4a of the Supporting Information) and electron diffraction (ED) patterns (Figure 3a). The amorphous phase exhibited a needle-like morphology different from that of the amorphous  $\text{CaCO}_3$  phase we have obtained before,<sup>30</sup> which may be due to the interior properties of the  $\text{BaCO}_3$  cell. After a reaction time of 30 min, the amorphous phase became denser and thicker (Figure 3b) and still retained the needle-like morphology. According to the ED patterns (inset of Figure 3b), the polymorph was still amorphous, but the transition tendency from amorphous to crystalline phase could be found through the obvious diffraction rings. The products obtained at 1 h were needles with a width of 40–50 nm and a length of 200–300 nm, which was obviously transited from the needle-like amorphous precursor phase. Weiner et al.<sup>33</sup> have demonstrated that amorphous calcium carbonate can be preoriented and transformed into certain nanoparticles for further aggregation. Herein, we suggest that the needle-like crystalline units were also transformed from the preoriented amorphous barium carbonate precursor.

At 2 h, we obtained shuttle-like particles in length of 8–10  $\mu\text{m}$ , similar to the aragonite particles transformed from the vaterite phase,<sup>35</sup> which indicated the similarity in structures of witherite and aragonite to some extent. It can be observed from the enlarged images (Figure 3e and inset of Figure 3d) that the shuttle-like particles were formed by stacking of needle-like crystalline units with a width of 40–50 nm in parallel, strongly suggesting that the shuttle-like particles were aggregated by the needle-like units formed earlier.

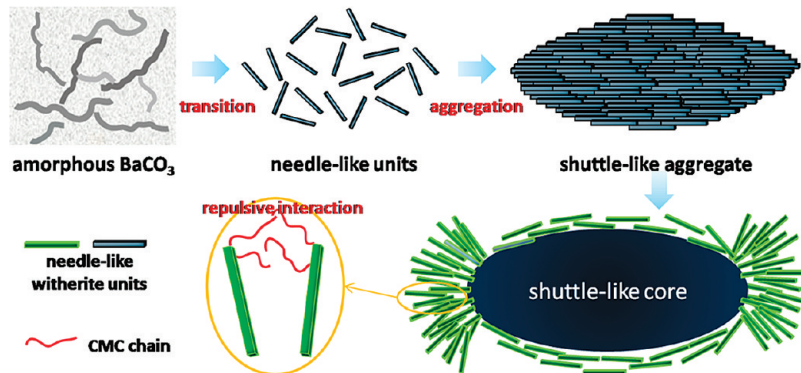
With the growing process, at 4 h, the dumbbell-like particles in a length of ca. 15  $\mu\text{m}$  were obtained (Figure 3f). We carefully examined the end of the dumbbell (Figure 3g) and found that it

was also composed of aggregated needle-like units. However, the stacking orientation between each unit is not so ordered as that in the shuttle-like particles formed at the early stage. There was an open angle between each needle-like unit. After 12 h of reaction, the final products were obtained and we examined the morphology of the particles through FESEM. The middle part of the particles were stacked needles in parallel (Figure 3i), while the end of the particles (shown in Figure 3k) were also stacked needles but not densely and in parallel, just with an open angle between each other. The connecting part between the end and the middle parts exhibited a transition in orientation (Figure 3j).

Recently, Colfen and Antonietti et al.<sup>11,12</sup> have developed the nonclassical crystallization theory, in which the fusion of the crystalline units and the extrusion of polymers from aggregates were involved. We have utilized the theory incorporating with the electrostatic repulsive interactions<sup>36,37</sup> between polyanion chains to successfully illustrate the formation of rosette-like calcite spheres induced by CMC.<sup>30</sup> Herein, based on the nonclassical crystallization theory and the simulation results of interactions between CMC segments and  $\text{BaCO}_3$ , we suggested the possible formation route of the above-mentioned dumbbell-like  $\text{BaCO}_3$  particles.

With  $\text{CO}_2$  and  $\text{NH}_3$  diffusing into the reaction system, the amorphous  $\text{BaCO}_3$  was first generated. Due to the interior properties of the witherite cell, the amorphous phase exhibited a needle-like morphology, which became denser and denser with time and soon transformed into a crystalline phase. The needle-like crystalline units were several hundreds of nanometers long with a width of 40–50 nm. Because the concentration of CMC is relatively low at 0.1 g/L, little amounts of polymer chains attached onto the units, so the needles could stack together in parallel (shoulder by shoulder) to form shuttle-like particles. Referring to the process in biological systems,<sup>7,38,39</sup> the polymers were likely to be extruded from the

**Scheme 2. Schematic Illustration of the Evolution of BaCO<sub>3</sub> Obtained under the Concentration of 0.1 g/L CMC and 0.01 M [Ba<sup>2+</sup>] Solution<sup>a</sup>**



<sup>a</sup>The relative size of the different species present in solution is not drawn to scale. See the text for more details.

aggregates during aggregation, which contributed to increasing the local polyanion concentration around the aggregates. These polymer chains extruded from aggregates then attached onto the subsequent units, in a way that chains preferred to attach onto the end of needle-like units but not the middle part, according to the simulation results we have calculated above. The electrostatic repulsive interactions among polyanions and the volume occupancy of polymer chains prevented the crystalline units from stacking in parallel but alternatively made the units stack with an open angle between each other, which is consistent with the conclusions we obtained during the formation of rosette-like calcite spheres.<sup>30</sup> Following such a process, the size of the particle increased and dumbbell-like BaCO<sub>3</sub> particles formed. The schematic illustration of the evolution was presented in Scheme 2.

**3.2.2. Morphological Evolution in CMC Solutions with Higher Concentrations.** We also investigated the morphological evolution when the polymer concentration is relatively higher. When the concentration was 0.5 g/L (Figures S5a and S5b of the Supporting Information), the amorphous precursor phase was spherical with a size of tens of nanometers and the final products depicted dumbbell-like morphology. With the concentration increasing to 1 g/L, it could be observed clearly from TEM images that the products obtained at 1 h were formed by aggregation of partially parallel needles with a width of 40–50 nm, as shown in Figure 4a and b and Figure S5c of the Supporting Information. ED patterns (inset of Figure 4a) indicated the transition state between amorphous and crystalline phases. When the CMC concentration increased to 5 g/L, the amorphous BaCO<sub>3</sub> precursor phase was spherical, probably due to the intersecting network formed in the higher polymer concentration, and the final products turned out to be twined spheres or spheres, also composed of needle-like units. It must be mentioned here that although the morphology of the precursor phase, and thus the detailed growth route including the aggregating manner under different concentrations, may have differences more or less, there was one common point existing in the production process of the aggregates under different concentrations: the products are all formed by aggregation of needle-like units with the same size.

X-ray diffraction patterns showed that the polymorphs of products obtained after 4 h of reaction are all witherite phase with typical planes (Figure 5). Before 4 h, XRD analysis could be hardly performed because of the small amount of the sample. The time-resolved XRD patterns indicated that

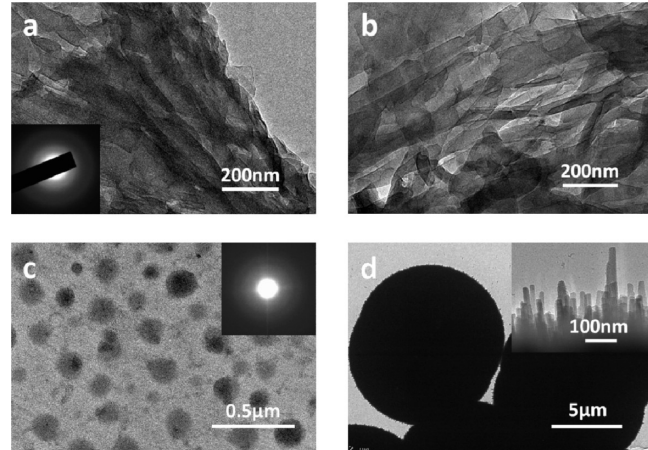


**Figure 4.** TEM images of BaCO<sub>3</sub> products obtained in 1 g/L CMC solutions and after a reaction time of 1 h (a, b) and in 5 g/L CMC solutions and after a reaction time of 30 min (c) and 12 h (d), respectively. The insets of parts a and c are ED patterns, and the inset of part d is an enlarged image.

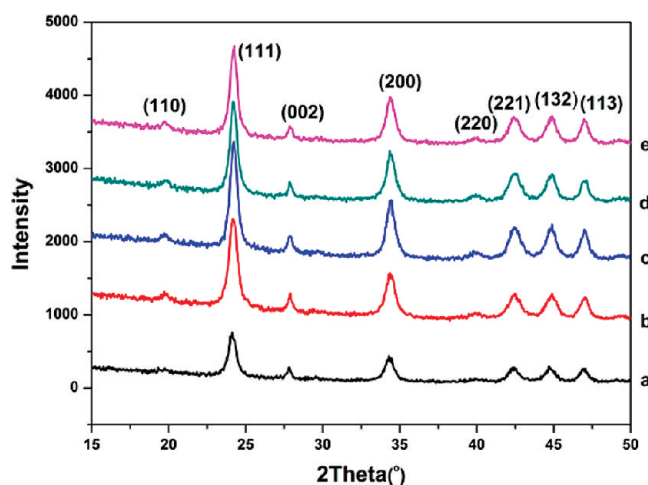


**Figure 5.** XRD patterns of BaCO<sub>3</sub> powders obtained by reaction of a 0.5 g/L CMC concentration at different intervals of 4 h (a), 6 h (b), 8 h (c), 10 h (d), and 12 h (e), respectively.

after 4 h the growth of aggregates did not go through any polymorph transformation. Actually, the products obtained at 4 h were already relatively stable and similar to the final

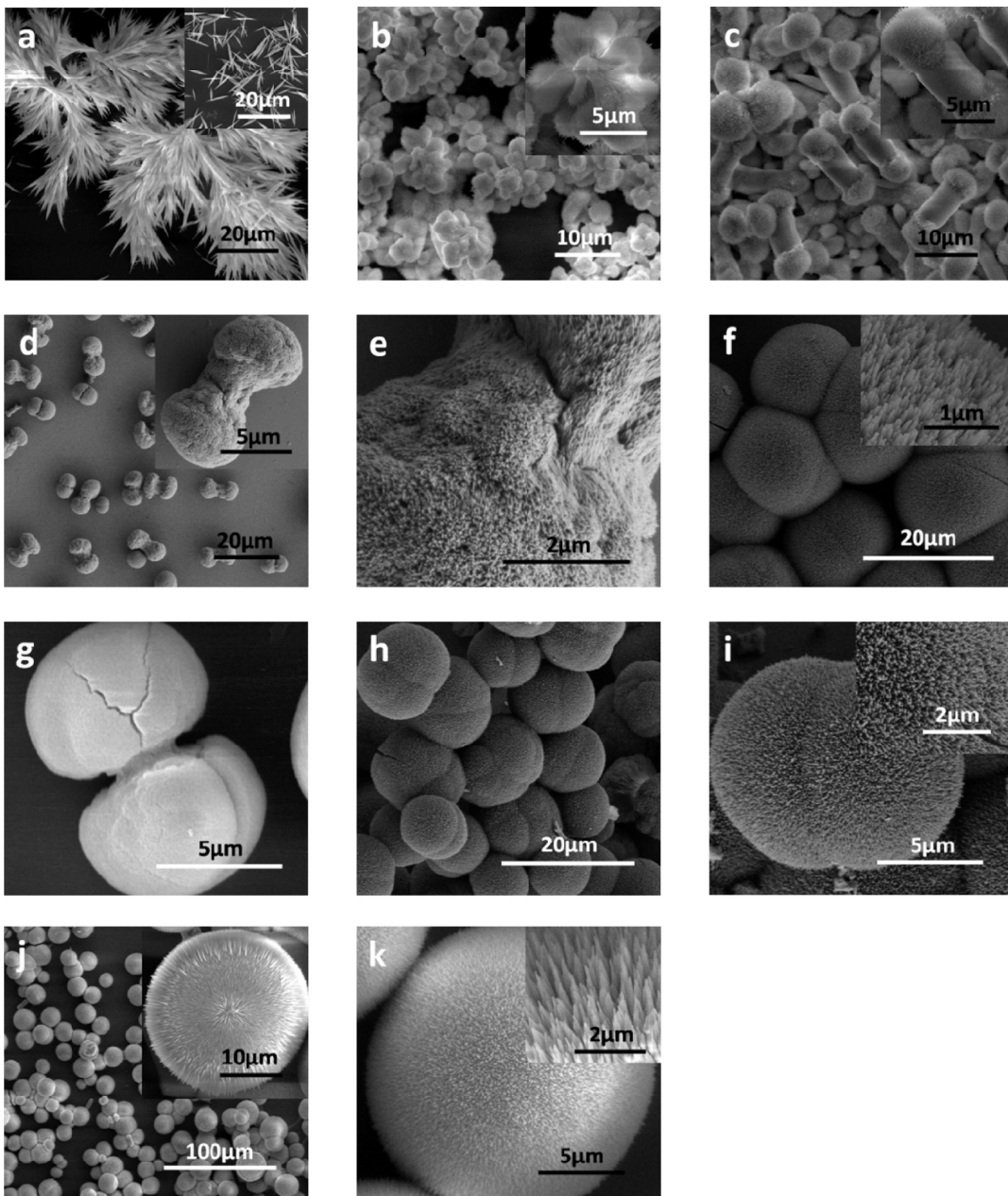


**Figure 6.** SEM and FESEM images of products obtained in CMC solutions after a reaction time of 12 h with a concentration of 0 (a), 0.01 g/L (b), 0.2 g/L (c), 0.5 g/L (d, e), 1 g/L (f, g), 5 g/L (h, i), and 10 g/L (j, k), respectively. The inset images are the enlarged pictures of corresponding particles.

products, which could also be proved by the electron micrograph results (Figure 3f and h).

**3.3. Controlling the Morphology of BaCO<sub>3</sub> Aggregates by Adjusting the Polymer Concentration.** Now that the formation mechanism of the BaCO<sub>3</sub> aggregates was clarified, we tried to control the morphology of products by affecting the aggregating method of needle-like crystalline units. By simply adjusting the CMC concentration in solution, we realized control over BaCO<sub>3</sub> morphologies from dumbbells to spheres. The final products obtained after 12 h of reaction under different CMC concentrations are presented in Figure 6. In all, with the polymer concentration increasing from 0 to 10 g/L (from Figure 6a to 6k), the morphologies of the particle undergo evolution from dendritic to dumbbell-like and then to twined spherical and spherical particles. In detail, when the reaction system contained no organic additives,

dendritic structures of BaCO<sub>3</sub> were generated (Figure 6a), similar to those reported in other works.<sup>2</sup> When little amount of CMC chains was added (0.01 g/L, Figure 6b), the morphology remained dendritic, similar to the structure of cauliflower, indicating that the effect of organics was not yet obvious. The morphology of particles obtained in 0.1 g/L CMC solution was dumbbell-like and was analyzed carefully above. When the concentration further increased to 0.2 g/L, dumbbell-like structures (Figure 6c) were also generated, but it should be noted that the diameter of the middle cylindrical part became slightly smaller, while the size of the end part of the dumbbell turned out to be relatively larger. When the concentration was 0.5 g/L (Figure 6d and e), the middle cylindrical part became shorter and thinner, with the size of the end part becoming larger. When we increased the concentration to 1 g/L, a small amount of dumbbell-like

**Scheme 3. Schematic Illustration of Different Structures of BaCO<sub>3</sub> Obtained under Different CMC Concentrations (See the Text for More Details)**

Concentration	Low, e.g. 0.1, 0.2 g/l	Medium, e.g. 0.5, 1 g/l	High, e.g. 5,10 g/l
Morphology			
Model			
Interaction between units			

particles was obtained (as Figure 6g shows), while a large proportion of twined spherical particles was generated, with the surfaces of spherical particles composed of needle-like units. As the polymer concentration continuously increased to 5 (Figure 6h and i) or, further, 10 g/L (Figure 6j and k), the twined spheres and the single spheres were obtained. From the SEM image of the cross section of the sphere (inset of Figure 6j), the spherical particle was grown from the central core by stacking of needles. In summary, there are no obvious differences between the size of the above particles (all in 10–20  $\mu\text{m}$ ), and it could be easily found that all particles obtained in different concentrations, no matter whether cauliflower, dumbbells, or spheres, are all constructed by the needle-like crystalline units with similar sizes.

According to the overlapped concentration of the CMC solution we calculated in our previous work ( $C^*$ , ca. 0.7 g/L),<sup>30</sup> we roughly divided the concentration into three regions: low concentration below  $C^*$  (e.g., 0.1, 0.2 g/L), medium concentration close to  $C^*$  (e.g., 0.5, 1 g/L), and high concentration (e.g., 5, 10 g/L) (Scheme 3). We have simulated the interactions between CMC segments and BaCO<sub>3</sub> units above and drawn the conclusion that the CMC chains favored attachment onto the end of the units. So at the low polymer concentration, needle-like units are favored to stack in parallel (shoulder by shoulder) to form shuttle-like particles because there was little amount of CMC chains attaching onto these units. Then due to the increase of the local polymer concentration around the shuttles, the subsequent needles stacked not completely in parallel but with an open angle between each other to form dumbbell-like particles, which was elucidated in the above text. When the concentration was close to the overlapped concentration, the amount of polymer chains adsorbed onto the units increased, including both those attaching on the end and those attaching in the middle part, so the electrostatic repulsive interaction and the volume repulsion between polyanions became stronger. Compared to the aggregation process at lower concentration, the tendency of units stacking in parallel decreased while stacking with an open angle increased. As a result, the cylindrical part of the dumbbell became shorter and thinner, and in comparison, the size of the end of the dumbbell increased. As the concentration further increased to be much higher than  $C^*$ , repulsive interactions between polyanions became so strong that the tendency for needles to stack in parallel was totally hindered; thus, the middle part of the product almost disappeared and all needle-like units stacked with an open angle between each other. In this situation, the

final products exhibited twined spherical morphology or spherical morphology. In total, with the concentration increasing, due to the increasing repulsive interaction between needle-like units, two effects emerged: both the length and the diameter of the cylindrical part of dumbbell-like particles decreased; the size of the end part increased. So we could realize control over the morphologies of BaCO<sub>3</sub> aggregates from dumbbells to twined spheres and spheres by simply altering the polymer concentration.

#### 4. Conclusion

Polymer chains were believed to have profound effects on the growth of inorganic crystals. Starting from the simulation of interactions between CMC chains and BaCO<sub>3</sub> supercells, we found that the polymer chains were favored to attach on the (111) face, that is, the end of the needle-like crystalline units. Then we traced the morphological evolution of dumbbell-like BaCO<sub>3</sub> products in CMC solution and suggested the polymer induced stacking mechanism of crystalline units based on the simulation results. Finally, we realized control over morphologies of products from dumbbell-like to twined spherical and spherical particles by simply adjusting the polymer concentration, in which we suggested that the overlapped concentration of polymer solution is an important factor. In all, we demonstrated here a systematic work on the morphological control of BaCO<sub>3</sub> aggregates mediated by CMC. The formation route of such carbonate aggregates is a typical self-assembly process affected by polymer additives. Incorporating the conclusions we have obtained in our previous works,<sup>30,31</sup> we thought that the growth process of minerals was affected by polymer additives in every period involving nucleation, growth, and aggregation. Depending on the reaction conditions, such as the reacting rate,<sup>31</sup> the degree of polymer effects performing on different processes is different. Herein, the effect of polymer on the aggregating process was clarified. Our present work not only provides a method to fabricate BaCO<sub>3</sub> particles with different structures and morphologies which can be used in many industrial sectors but also sheds light on the mechanistic interpretation of biomimetic mineralization induced by polymer additives.

**Acknowledgment.** We gratefully acknowledge the financial support of the National Science Foundation of China (NSFC) (No. 20934002, 20774022) and the National Basic Research Program of China (2009CB930000).

**Supporting Information Available:** Simulation results of the lattice cell and TEM images of the obtained BaCO<sub>3</sub> products. This material is available free of charge via the Internet at <http://pubs.acs.org>.

## References

- (1) Wang, T. X.; Xu, A. W.; Colfen, H. *Angew. Chem., Int. Ed.* **2006**, *45*, 4451–4455.
- (2) Yu, S. H.; Colfen, H.; Xu, A. W.; Dong, W. F. *Cryst. Growth Des.* **2004**, *4*, 33–37.
- (3) Colfen, H.; Mann, S. *Angew. Chem., Int. Ed.* **2003**, *42*, 2350–2365.
- (4) Whitesides, G. M.; Grzybowski, B. *Science* **2002**, *295*, 2418–2421.
- (5) Mann, S.; Ozin, G. A. *Nature* **1996**, *382*, 313–318.
- (6) Xu, A. W.; Ma, Y. R.; Colfen, H. *J. Mater. Chem.* **2007**, *17*, 415–449.
- (7) Addadi, L.; Joester, D.; Nudelman, F.; Weiner, S. *Chem.—Eur. J.* **2006**, *12*, 981–987.
- (8) Tugulu, S.; Harms, M.; Fricke, M.; Volkmer, D.; Klok, H. A. *Angew. Chem., Int. Ed.* **2006**, *45*, 7458–7461.
- (9) Hosoda, N.; Kato, T. *Chem. Mater.* **2001**, *13*, 688–693.
- (10) Mann, S. In *Biomimetic Principles and Concepts in Bioinorganic Materials Chemistry*; Oxford University Press: Oxford, 2001; pp 45–51.
- (11) Kulak, A. N.; Iddon, P.; Li, Y. T.; Armes, S. P.; Colfen, H.; Paris, O.; Wilson, R. M.; Meldrum, F. C. *J. Am. Chem. Soc.* **2007**, *129*, 3729–3736.
- (12) Wang, T. P.; Antonietti, M.; Colfen, H. *Chem.—Eur. J.* **2006**, *12*, 5722–5730.
- (13) Yu, S. H.; Colfen, H. *J. Mater. Chem.* **2004**, *14*, 2124–2147.
- (14) Cheng, C.; Shao, Z. Z.; Vollrath, F. *Adv. Funct. Mater.* **2008**, *18*, 2172–2179.
- (15) Politis, Y.; Mahamid, J.; Goldberg, H.; Weiner, S.; Addadi, L. *CrystEngComm* **2007**, *9*, 1171–1177.
- (16) Arias, J. L.; Fernandez, M. S. *Chem. Rev.* **2008**, *108*, 4475–4482.
- (17) Zhu, J. H.; Yu, S. H.; Xu, A. W.; Colfen, H. *Chem. Commun.* **2009**, 1106–1108.
- (18) Guo, X. H.; Yu, S. H. *Cryst. Growth Des.* **2007**, *7*, 354–359.
- (19) Yu, S. H.; Colfen, H.; Antonietti, M. *J. Phys. Chem. B* **2003**, *107*, 7396–7405.
- (20) Yu, S. H.; Colfen, H.; Tauer, K.; Antonietti, M. *Nat. Mater.* **2005**, *4*, 51–55.
- (21) Harding, J. H.; Duffy, D. M.; Sushko, M. L.; Rodger, P. M.; Quigley, D.; Elliott, J. A. *Chem. Rev.* **2008**, *108*, 4823–4854.
- (22) Rahaman, A.; Grassian, V. H.; Margulis, C. J. *J. Phys. Chem. C* **2008**, *112*, 2109–2115.
- (23) Wang, X. W.; Han, Y. S.; Lin, L. W.; Fuji, M.; Endo, T.; Watanabe, H.; Takahashi, M. *Model. Simul. Mater. Sci. Eng.* **2008**, *16*, 035006.
- (24) Hadicke, E.; Rieger, J.; Rau, I. U.; Boeckh, D. *Phys. Chem. Chem. Phys.* **1999**, *1*, 3891–3898.
- (25) Navarro, R. R.; Tatsumi, K.; Sumi, K.; Matsumura, M. *Wat. Res.* **2001**, *35*, 2724–2730.
- (26) Akin, B.; Oner, M.; Bayram, Y.; Demadis, K. D. *Cryst. Growth Des.* **2008**, *8*, 1997–2005.
- (27) Backfolk, K.; Lagergård, S.; Rosenholm, J. B.; Eklund, D. *J. Colloid Interface Sci.* **2002**, *248*, 5–12.
- (28) Barbucci, R.; Magnani, A.; Consumi, M. *Macromolecules* **2000**, *33*, 7475–7480.
- (29) Li, W.; Sun, B. J.; Wu, P. Y. *Carbohydr. Polym.* **2009**, *78*, 454–461.
- (30) Li, W.; Wu, P. Y. *CrystEngComm* **2009**, *11*, 2466–2474.
- (31) Li, W.; Yu, Q. S.; Wu, P. Y. *Green Chem.* **2009**, *11*, 1541–1549.
- (32) Kamburova, K.; Radeva, T. *J. Colloid Interface Sci.* **2007**, *313*, 398–404.
- (33) Weiner, S.; Sagi, I.; Addadi, L. *Science* **2005**, *309*, 1027–1028.
- (34) Addadi, L.; Raz, S.; Weiner, S. *Adv. Mater.* **2003**, *15*, 959–970.
- (35) Shen, Q.; Wang, L. C.; Huang, Y. P.; Sun, J. L.; Wang, H. H.; Zhou, Y.; Wang, D. *J. Phys. Chem. B* **2006**, *110*, 23148–23153.
- (36) Kuther, J.; Seshadri, R.; Nelles, G.; Assenmacher, W.; Butt, H. J.; Mader, W.; Tremel, W. *Chem. Mater.* **1999**, *11*, 1317–1325.
- (37) Kuther, J.; Seshadri, R.; Tremel, W. *Angew. Chem., Int. Ed.* **1998**, *37*, 3044–3047.
- (38) Rousseau, M.; Lopez, E.; Coute, A.; Mascarel, G.; Smith, D. C.; Naslain, R.; Bourrat, X. *J. Struct. Biol.* **2005**, *149*, 149–157.
- (39) Song, F.; Soh, A. K.; Bai, Y. L. *Biomaterials* **2003**, *24*, 3623–3631.